Fungal gasdermin-like proteins are controlled by proteolytic cleavage

Corinne Clavé[a,1], Witold Dyrka[b], Elizabeth A. Turcotte[c], Alexandra Granger-Farbos[a], Léa Ibarlosa[a], Benoît Pinson[d], Russell E. Vance[c,e,f,g], Sven J. Saupe[a], and Asen Daskalov[a,1]

[a]UMR 5095, CNRS, Non-self Recognition in Fungi, Institut de Biochimie et Génétique Cellulaires, Université de Bordeaux, 33077 Bordeaux, France; [b]Politechnika Wrocławska, Wydział Podstawowych Problemów Techniki, Katedra Inżynierii Biomedycznej, 50-370 Wrocław, Poland; [c]Division of Immunology and Pathogenesis, Department of Molecular and Cell Biology, University of California, Berkeley, CA 94720; [d]UMR 5095, CNRS, Genetics of Metabolic Pathways, Institut de Biochimie et Génétique Cellulaires, Université de Bordeaux, 33077 Bordeaux, France; [e]HHMI, University of California, Berkeley, CA 94720; [f]Immunotherapeutics and Vaccine Research Initiative, University of California, Berkeley, CA 94720; and [g]Cancer Research Laboratory, University of California, Berkeley, CA 94720

Edited by Zhijian Chen, Department of Molecular Biology, The University of Texas Southwestern Medical Center, Dallas, TX; received May 20, 2021; accepted January 4, 2022

Gasdermins are a family of pore-forming proteins controlling an inflammatory cell death reaction in the mammalian immune system. The pore-forming ability of the gasdermin proteins is released by proteolytic cleavage with the removal of their inhibitory C-terminal domain. Recently, gasdermin-like proteins have been discovered in fungi and characterized as cell death–inducing toxins in the context of conspecific non-self–discrimination (allorecognition). Although functional analogies have been established between mammalian and fungal gasdermins, the molecular pathways regulating gasdermin activity in fungi remain largely unknown. Here, we characterize a gasdermin-based cell death reaction controlled by the *het-Q* allorecognition genes in the filamentous fungus *Podospora anserina*. We show that the cytotoxic activity of the HET-Q1 gasdermin is controlled by proteolysis. HET-Q1 loses a ∼5-kDa C-terminal fragment during the cell death reaction in the presence of a subtilisin-like serine protease termed HET-Q2. Mutational analyses and successful reconstitution of the cell death reaction in heterologous hosts (*Saccharomyces cerevisiae* and human 293T cells) suggest that HET-Q2 directly cleaves HET-Q1 to induce cell death. By analyzing the genomic landscape of *het-Q1* homologs in fungi, we uncovered that the vast majority of the gasdermin genes are clustered with protease-encoding genes. These HET-Q2–like proteins carry either subtilisin-like or caspase-related proteases, which, in some cases, correspond to the N-terminal effector domain of nucleotide-binding and oligomerization-like receptor proteins. This study thus reveals the proteolytic regulation of gasdermins in fungi and establishes evolutionary parallels between fungal and mammalian gasdermin-dependent cell death pathways.

gasdermin | fungi | regulated cell death | innate immunity | proteolysis

Spatiotemporally localized, regulated cell death (RCD) prevents cytoplasmic mixing and heterokaryon formation between conspecific individuals in fungi (1, 2). The cell death reaction limits the transmission of mycoviruses and other deleterious replicons, thus representing a defense reaction akin to an immune response (3, 4). The molecular characterization of cell death pathways, regulating conspecific non-self–discrimination (allorecognition) in fungi, has revealed evolutionary relations to cell death pathways operating in mammalian innate immunity, notably necroptosis and pyroptosis (5, 6). The extent of the conservation of these pathways is gradually revealed as the characterization of fungal RCD pathways progresses.

Proteolytic cleavage is a general mechanism for regulation of programmed cell death and RCD in metazoans and plants (7). In mammals, a family of cysteine-aspartic proteases (caspases) controls cellular suicide pathways like apoptosis and pyroptosis (8, 9). The latter represents a highly inflammatory, lytic cell death reaction playing a central role in mammalian innate immunity (10, 11). Pyroptotic cell death is induced by proinflammatory caspases (caspase-1, -4, -5, and -11), which cleave a protein termed gasdermin D (GSDMD) (12, 13). The cleavage of GSDMD liberates the cytotoxic N-terminal domain of the protein (GSDMD-NT) from the inhibitory C-terminal domain, and the processed GSDMD-NT disrupts the integrity of the plasma membrane by pore formation (14–17). GSDMD belongs to a protein family comprising six members in humans (gasdermin A [GSDMA], gasdermin B [GSDMB], gasdermin C, gasdermin E [GSDME, also DFNA5], and PJVK [also DFNB59]) (18). Proteolytic cleavage has been shown to regulate the cytotoxic activity of other members of the gasdermin family, specifically of GSDME (19) and GSDMB (20). While the regulation of GSDME is caspase-3 dependent (19, 21), it has recently been reported that GSDMB is proteolytically activated by a serine protease termed granzyme A (GZMA) (20).

Gasdermin-like proteins are abundant and widespread in fungi, with some species encoding more than 20 gasdermin homologs in their genomes (22). It has recently been established that a fungal gasdermin-like protein controls cell death in the context of allorecognition. The coexpression of antagonistic

Significance

The recent discovery of gasdermin-like proteins in fungi have brought to light that this family of pore-forming proteins controls cell death in two of the major eukaryotic kingdoms, fungi and mammals. Yet the regulation of cytotoxicity of the fungal gasdermins and their molecular pathways remain uncharacterized. Here, we describe the regulation through proteolytic cleavage of the fungal gasdermin HET-Q1 and uncover that a majority of fungal gasdermins are genomically clustered with protease-encoding genes. Some of these genes encode proteins with caspase-related domains and/or are members of a family of immune receptors in mammals and plants. Overall, this work contributes toward our understanding of the evolution of gasdermin-dependent cell death, enlightening multiple evolutionary parallels between signaling pathways in mammals and fungi.

Author contributions: C.C., W.D., S.J.S., and A.D. designed research; C.C., W.D., E.A.T., A.G.-F., L.I., B.P., and A.D. performed research; C.C., W.D., E.A.T., A.G.-F., L.I., B.P., R.E.V., S.J.S., and A.D. analyzed data; and A.D. wrote the paper.

The authors declare no competing interest.

This article is a PNAS Direct Submission.

See online for related content such as Commentaries.

[1]To whom correspondence may be addressed. Email: corinne.clave@ibgc.cnrs.fr or asen.daskalov@u-bordeaux.fr.

This article contains supporting information online at http://www.pnas.org/lookup/suppl/doi:10.1073/pnas.2109418119/-/DCSupplemental.

Published February 8, 2022.

alleles of the *rcd-1* gene (regulator of cell death) triggers rapid, lytic cell death in asexual spores and hyphae of the model ascomycete *Neurospora crassa* (22). RCD-1 is a distant homolog of the cytotoxic pore-forming GSDMD-NT domain and, like gasdermin, induces cell death by targeting the plasma membrane while forming oligomers (6). However, despite the uncovered functional similarities between the mammalian gasdermins and fungal RCD-1 gasdermin–like protein, in the latter case, cytotoxic activity is not dependent on proteolytic activation but results instead from the interaction of antagonistic RCD-1 variants.

Here, we characterized the fungal gasdermin HET-Q1 from *Podospora anserina* and report that its cytotoxic activity is regulated through proteolytic cleavage by a subtilisin-like serine protease named HET-Q2. *het-Q1* and *het-Q2* are idiomorphic genes (they represent alternate alleles of the same *het-Q* locus but are totally unrelated in sequence) and regulate cell death in the context of heterokaryon formation (somatic fusions between different strains). We demonstrated that a ∼5-kDa (kilodaltons) C-terminal fragment is cleaved from HET-Q1 in the presence of HET-Q2. Expression of a truncated variant—HET-Q1(1-238)—was sufficient to reduce cell viability, while a point mutant—HET-Q1-F238A—preventing proteolytic cleavage of the fungal gasdermin abolished its cytotoxicity. Catalytically inactive mutants of the HET-Q2 protease were equally unable to produce cell death when coexpressed with HET-Q1. The *het-Q1*/*het-Q2* RCD reaction can be reconstructed in the distant heterologous yeast host *Saccharomyces cerevisiae* and human 293T cells, which strongly suggests that HET-Q2 removes directly the C-terminal inhibitory end of the gasdermin HET-Q1 to induce cell death. Importantly, in silico analyses of the genomic landscape of *het-Q1* homologs revealed that the fungal gasdermin genes are, in the vast majority of cases, the genomic neighbors of protease-encoding *het-Q2*–like genes. In addition, ∼20% of these protease-encoding neighbors carry a predicted caspase-like domain. Our work indicating that members of the gasdermin family in fungi are regulated through proteolytic cleavage reveals a remarkable evolutionary conservation of regulated cell death pathways in eukaryotes.

Results

RCD during *het-Q* Allorecognition Is Controlled by Idiomorphic Genes. The *het-Q* locus is one of the last uncharacterized allorecognition loci in *P. anserina* (23). *P. anserina* strains either belong to the *het-Q1* or *het-Q2* genotype. The cellular fusions between strains from different *het-Q* genotypes are abortive and trigger RCD, which translates with the appearance of a "barrage" (demarcation line) between such strains (Fig. 1*A* and *SI Appendix*, Fig. S1). The *het-Q* locus has been genetically located on chromosome 7 (24). To identify the precise genetic determinants controlling *het-Q* RCD, we analyzed the genetic distance between *het-Q* and the *PaATG1* locus (Pa_7_10890) situated on the same chromosome (25). We measured ∼2.5% of recombination between *het-Q* and *PaATG1*, which corresponds to ∼60 kbp (kilobase pair) in estimated physical distance between the two genes. We thus undertook a positional cloning approach with a DNA library of cosmids and plasmids from a *het-Q1* strain, covering a region of ∼100 kbp around the *PaATG1* gene (*SI Appendix*, Fig. S2 and Tables S1–S3). The cosmid and plasmid clones were transformed into protoplasts of the incompatible *het-Q2* genetic background. Since the coexpression of *het-Q1* and *het-Q2* is lethal, it is expected that clones bearing *het-Q1* show reduced transformation efficiency in this background (*SI Appendix*, Fig. S2 and Tables S1 and S2). Only constructs bearing the Pa_7_10775 gene showed reduced transformation efficiencies specifically in the *het-Q2* genetic background (*SI Appendix*, Fig. S2 and Tables S3 and S4). These experiments suggest that Pa_7_10775 is allelic to *het-Q1*. We replaced the Pa_7_10775 gene with a *nat1* cassette (nourseothricin resistance marker), producing a Δ*Pa_7_10775* strain, which showed wild-type growth and fertility. The Δ*Pa_7_10775* strain no longer produced a barrage reaction with a *het-Q2* strain, indicating that the RCD reaction is abolished (Fig. 1*A*). The ectopic reintroduction of Pa_7_10775 into the Δ*Pa_7_10775* background restored the barrage reaction to *het-Q2* (Fig. 1 *A* and *B*). These results indicate that Pa_7_10775 is *het-Q1*. The Δ*Pa_7_10775* strain was thus designated Δ*het-Q*.

Next, we amplified the same locus from a *het-Q2* strain using primers located in the ORFs (open reading frame) flanking *het-Q1* (Pa_7_10775), Pa_7_10770 and Pa_7_10780 (*SI Appendix*, Fig. S2). The cloned corresponding PCR fragment showed reduced transformation efficiency in the *het-Q1* background, while the transformation efficiencies into the *het-Q2* or Δ*het-Q* backgrounds were at levels similar to that with the empty vector (*SI Appendix*, Fig. S2 and Table S4). Δ*het-Q* strains transformed with this PCR fragment acquired the *het-Q2* phenotype and triggered RCD with a *het-Q1* tester strain (Fig. 1). The *het-Q* locus situated between the Pa_7_10770 and Pa_7_10780 ORFs is totally dissimilar between the *het-Q1* and *het-Q2* strains and varies in length in the two backgrounds with 1.6 kbp and 2.4 kbp, respectively (Fig. 1*C*). The *het-Q1* and *het-Q2* genes are thus best described as idiomorphs rather than classical alleles (26).

***het-Q1* Encodes a Gasdermin Homolog and *het-Q2* a Putative Serine Protease.** The *het-Q1* gene encodes a 278-amino-acid-long protein, HET-Q1, which belongs to the same protein family as RCD-1 from *N. crassa* (6) and thus is a fungal gasdermin-like protein (*SI Appendix*, Fig. S3). We confirmed the homology between HET-Q1 and mammalian gasdermins using the HHPred suite (27). The in silico analyses uncovered two regions of higher sequence conservation between HET-Q1, GSDMD-NT, and GSDMA3-NT, detected around residues 148 to 155 and 210 to 217 as previously reported for the RCD-1 protein (*SI Appendix*, Fig. S3). The HET-Q1 protein was also modeled with AlphaFold2 (28). The structural model showed a high-confidence twisted β-sheet core, and structural comparisons using Dali (29) identified Gasdermin-A3 (and other gasdermins) as the closest structural relatives to the generated model (*SI Appendix*, Fig. S4 and Table S5). The analysis confirms further the evolutionary relation between HET-Q1 and gasdermins.

The *het-Q2* ORF (GenBank: MZ576188) encodes a 366-amino-acid-long protein. HET-Q2 shows homology to subtilisin-like serine proteases of the S8 family (*SI Appendix*, Fig. S3). No signal peptide was detected in HET-Q2, which suggests that the predicted protease is not secreted. Based on sequence alignments and homology modeling, the amino acid residues D35, H105, and S266 of HET-Q2 were identified as constituting the catalytic triad of the putative protease. HET-Q2 lacks an N-terminal propeptide inhibitor domain (i.e., I9 domain) typically found in S8 subtilisin proteases (30).

HET-Q2–Dependent Proteolytic Cleavage of HET-Q1 Triggers Cell Death. Considering the homology with mammalian gasdermins and the fact that these cell death–inducing proteins are activated by proteolytic cleavage, we reasoned that the HET-Q1/HET-Q2 cell death reaction might result from the proteolytic cleavage of the HET-Q1 gasdermin by the HET-Q2 serine protease. To test this hypothesis, we produced the N-terminally V5-tagged HET-Q1 allelic variant (referred as V5-HET-Q1 or V5-Q1), which was functional and induced cell death at wild-type levels (*SI Appendix*, Fig. S5). We then explored the proteolytic reaction by mixing crude cell extracts (cytoplasmic content) of strains expressing V5-tagged HET-Q1 with extracts from a *het-Q2* strain or from the Δ*het-Q* strain. Lysates mixtures (1:1 ratio) were incubated for up to 30 min (25 °C). At the initial time point (at 0 min) in both reaction mixtures

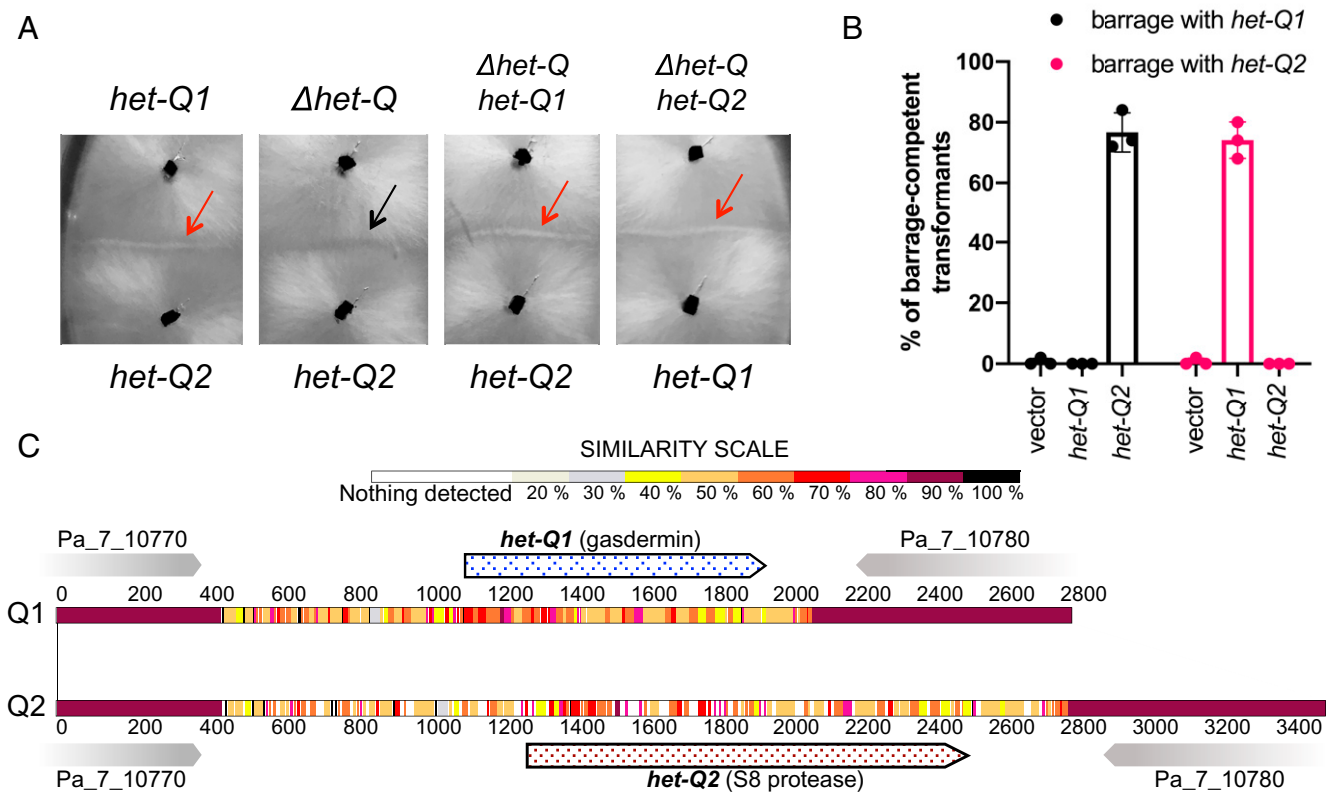

Fig. 1. Gene idiomorphs *het-Q1* (gasdermin homolog) and *het-Q2* (S8 serine protease) define an RCD system in the context of heterokaryon incompatibility (allorecognition) in *P. anserina*. (*A*) Cell death between *P. anserina* strains of antagonistic *het-Q1* and *het-Q2* genotypes manifests with the appearance of a "barrage" reaction between the fungal colonies (red arrows). The deletion of the *het-Q1* gene (Pa_7_10775) produces a Δ*het-Q* strain (we term it Δ*het-Q* because the *het-Q1* and *het-Q2* strains are isogenic with the exception of the *het-Q* locus) and abolishes the cell death reaction (barrage formation) with a *het-Q2* strain (black arrow). Reintroduction of *het-Q1* in a Δ*het-Q* strain restores the barrage reaction with a *het-Q2* tester strain, while introduction of *het-Q2* in the Δ*het-Q* background procures the ability to the transformants to produce a barrage reaction with a *het-Q1* tester strain. (*B*) The quantification of *het-Q1*/*het-Q2* cell death by testing transformants (from Δ*het-Q* genotype), obtained by introducing *het-Q1*, *het-Q2*, or an empty vector for the ability to produce a barrage reaction with a *het-Q1* or a *het-Q2* tester strain. The experiments were performed in triplicate with 50 transformants tested per experiment. Empty vector has been used as a negative control. (*C*) Graphic representation of the *het-Q* locus as found in strains from the *het-Q1* (Q1) and the *het-Q2* genotypes (Q2). Shown is an alignment of the *het-Q* locus from a *het-Q1* and *het-Q2* strain. Sequence similarity at nucleotide level is color-coded. Regions encoding the idiomorphic genes show low sequence similarity (in 40 to 60% range), while regions encoding the neighboring genes (Pa_7_10770 and Pa_7_10780) show sequence similarity above 90% between the two genotypes.

(V5-Q1 + Q2 and V5-Q1 + ΔQ), the V5-tagged HET-Q1 protein was detected by Western blot at the expected molecular weight (~32 kDa) (Fig. 2*A*). The molecular weight of HET-Q1 remained unchanged in the mixture of crude lysates from the *v5-het-Q1* and Δ*het-Q* strains (V5-Q1 + ΔQ) (Fig. 2*A*). However, in the presence of HET-Q2 (V5-Q1 + Q2 mixture), we observed a progressive decrease in the amount of full-length HET-Q1 with a correlated appearance of a fragment of lower molecular weight (~28 kDa) corresponding to the N-terminal part of the HET-Q1 protein (Fig. 2*A*). We concluded that in the presence of the HET-Q2 serine protease, HET-Q1 is proteolytically processed, and a ~5-kDa C-terminal fragment (or domain) is cleaved from the protein.

To investigate whether the proteolytic cleavage activates the cytotoxicity of HET-Q1, we produced four truncated protein variants, removing short fragments in ~15-amino-acid increments from the C-terminal end of the protein. The truncations were introduced in the Δ*het-Q* strain, and the number of viable transformants was quantified (Fig. 2*B*). Three of the tested truncations [HET-Q1(1-261), HET-Q1(1-247), and HET-Q1(1-218)] showed normal levels of transformation efficiency, while the fourth truncation—HET-Q1(1-233)—resulted in a significant decrease in the number of viable transformants (Fig. 2*B*). Western blot analyses confirmed that the HET-Q1(1-233) truncation is of similar molecular weight to processed HET-Q1 (Fig. 2*C*). Noteworthy, among the truncation constructs, only strains expressing HET-Q1(1-261) produce barrage with a HET-Q2–expressing strain (*SI Appendix*, Fig. S5). These results suggest that some of the truncations impact the N-terminal cytotoxic domain of HET-Q1 and/or prevent the activation of the toxin by the protease. We concluded that the removal of the last 45 amino acid residues of HET-Q1—producing the HET-Q1(1-233) fragment—leads to an increased cytotoxicity of HET-Q1. In addition, we performed size-exclusion chromatography with cellular extracts. While unprocessed HET-Q1 elutes in low molecular weight fractions, we found that in mixtures containing HET-Q1 and HET-Q2 (Q1+Q2), proteolytically processed HET-Q1 elutes in the void fraction. This result suggests that the proteolytic cleavage induces a transition from the monomeric toward the multimeric state of the fungal toxin, similar to members of the gasdermin family in mammals (Fig. 2*D*) (18).

Next, we undertook to identify amino acid residues important for the proteolytic cleavage of HET-Q1 and replaced individual residues with alanines in the region where the cleavage occurs. We generated a set of seven HET-Q1 mutants, encompassing the region from residues G234 to G241 of HET-Q1 (Fig. 2*E*), and tested the ability of the mutants to induce cell

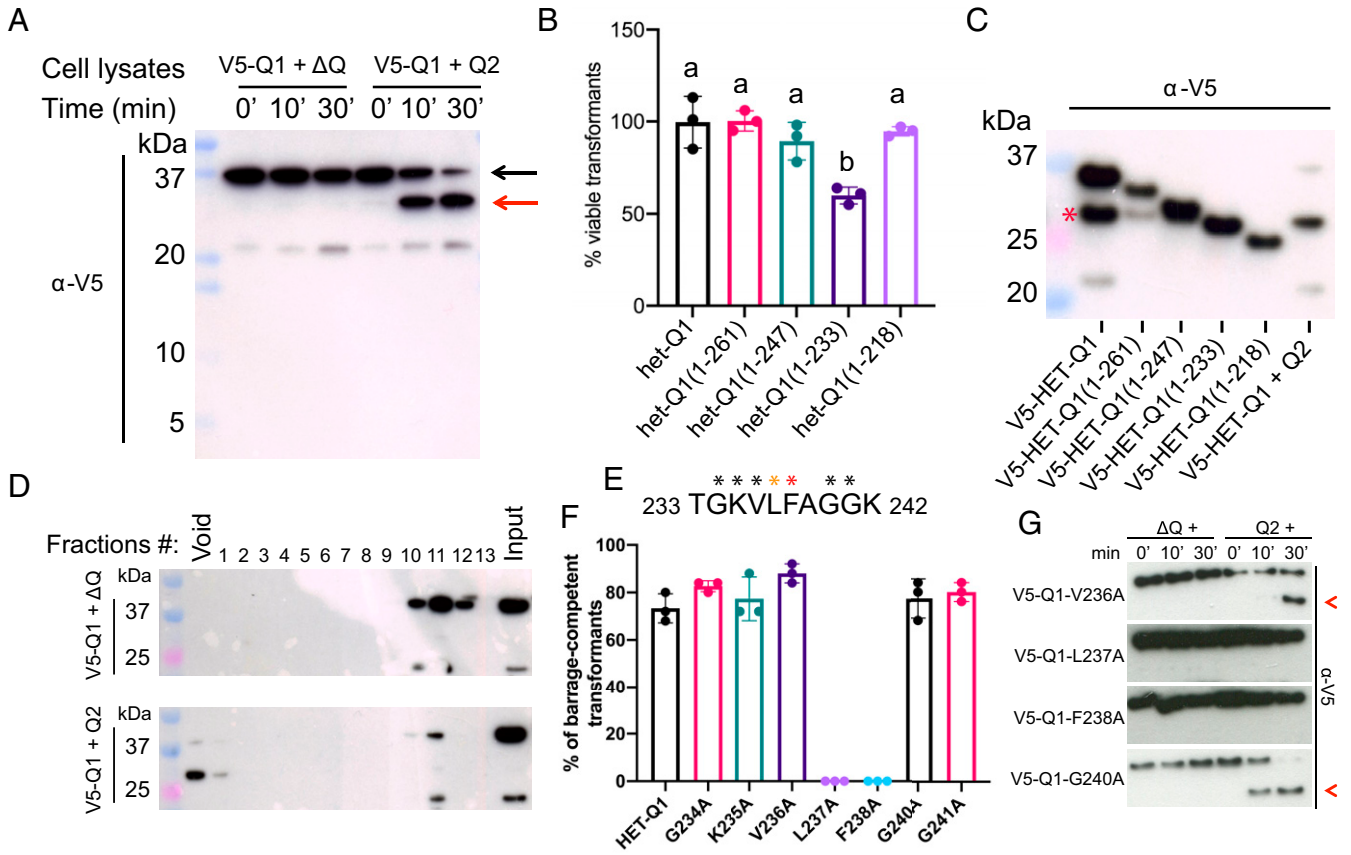

Fig. 2. HET-Q2–dependent proteolytic cleavage of the gasdermin-like protein HET-Q1 induces cell death in *P. anserina*. (*A*) Western blot showing accumulation of processed V5-HET-Q1 (V5-Q1) in a *het-Q2*–dependent manner. Crude cell lysates from a V5-HET-Q1–expressing strain were mixed and incubated (for up to 30 min) with cell extracts from a Δ*het-Q* strain (V5-Q1 + ΔQ) or from a *het-Q2* strain (V5-Q1 + Q2). In the first reaction (V5-Q1 + ΔQ), V5-HET-Q1 remained unprocessed and appeared as a single band at the expected size for the full-length protein (~32 kDa) (black arrow). However, when mixed with extracts from a *het-Q2* strain (V5-Q1 + Q2), a smaller V5-HET-Q1 fragment (27 to 30 kDa) (red arrow) appears and accumulates in time, while the amount of full-length protein progressively decreases. (*B*) Quantification of transformation viability of Δ*het-Q* transformants with truncated *het-Q1* alleles. Four truncations of *het-Q1* were introduced into Δ*het-Q* protoplasts and number of viable transformants counted. Three of the truncations [*het-Q1(1-261)*, *het-Q1(1-247)*, and *het-Q1(1-218)*] produced wild-type levels of viable transformants. Transformations with the fourth truncation—*het-Q1(1-233)*—resulted in ~45% reduction of viable transformants. Experiments were performed in triplicate. *P* value (a ≠ b) < 0.01, one-way ANOVA with Tukey's multiple comparisons test. (*C*) Western blot of full-length and truncated V5-HET-Q1 variants. Cytotoxic V5-HET-Q1(1-233) is of similar molecular size to processed V5-HET-Q1 in mixtures of cell extracts (V5-HET-Q1 + Q2). Protein bands corresponding to unspecific proteolysis because of high levels of protein expression are shown with red asterisk. (*D*) Polyacrylamide gel electrophoresis and Western blot of fast protein liquid chromatography fractions of crude cell extracts mixtures. Cell extracts containing V5-HET-Q1 were mixed with cell extracts from a Δ*het-Q* strain (V5-Q1 + ΔQ) (*Top*) or from a *het-Q2* strain (V5-Q1 + Q2) (*Bottom*). Processed V5-HET-Q1 in mixtures containing the HET-Q2 protease elutes in the void volume containing protein aggregates of high molecular weight (above 1 MDa [megadalton]), while unprocessed V5-HET-Q1 elutes in fractions corresponding to proteins with lower molecular weight, close to that of monomeric V5-HET-Q1 (~32 kDa). The mixtures at zero minutes of incubation were used as "input." (*E*) Protein sequence of HET-Q1(233-242). Amino acid residues substituted with alanine residues are marked with asterisks. Black asterisks indicate residues, which substitution did not impact the cell death reaction. Red asterisk indicates that the substitution abolishes the cell death reaction, and yellow asterisk indicates that it impacts partially cell death. (*F*) Quantification of barrage-inducing transformants expressing mutant V5-HET-Q1 variants. The experiments were performed in triplicate with 25 tested transformants per experiment. Mutant variants HET-Q1(L237A) and HET-Q1(F238A) are significantly affected in their cell death–inducing ability (*P* value < 0.0001, one-way ANOVA with Tukey's multiple comparisons test). (*G*) Western blots of V5-HET-Q1 mutant variants in cell extract mixtures containing HET-Q2 protease (Q2 +) or without (ΔQ +). Mutations affecting the cell death reaction (V5-Q1-L237A and V5-Q1-F238A) prevent proteolytic cleavage of HET-Q1. Proteolytically processed mutants (V5-Q1-V236A and V5-Q1-G240A) are shown with red arrowheads.

death with a strain expressing HET-Q2 (Fig. 2*F*). The majority of HET-Q1 mutants were not affected in their ability to induce cell death. Only strains expressing HET-Q1-L237A and HET-Q1-F238A were unable to produce barrage with the *het-Q2* strain (Fig. 2*F*). However, after prolonged contact between transformants expressing HET-Q1-L237A and the *het-Q2* strain, we observed the formation of attenuated barrages, suggesting that the mutation affects the cell death reaction only partially. We then probed whether the proteolytic cleavage of the HET-Q1-L237A and HET-Q1-F238A mutants occurs in the presence of HET-Q2 (Fig. 2*G*). Crude cellular extracts from transformants expressing the HET-Q1 mutant variants were mixed in a 1:1 ratio with cellular extracts from a Δ*het-Q* strain or *het-Q2* strain and incubated for up to 30 min. Mutations affecting the cell death reaction (L237A and F238A) were found to equally affect the proteolytic cleavage of HET-Q1. The two mutant variants (HET-Q1-L237A and HET-Q1-F238A) remained unprocessed even after 30 min in the presence of HET-Q2 (Fig. 2*G*). Mutant HET-Q1 variants that did not affect the cell death reaction (V236A and G240A) did not abolish the proteolytic cleavage of HET-Q1 and were processed after 30 min in the presence of HET-Q2 (Fig. 2*G*). We concluded from these experiments that the amino acid residues L237 and F238 are important for the proteolytic cleavage of

HET-Q1 and could be integral to the cleavage site. To investigate further the latter possibility, we generated three HET-Q1 truncations [HET-Q1(1-237), HET-Q1(1-238), and HET-Q1(1-239)] and tested for their ability to reduce cell viability post-transformation (*SI Appendix*, Fig. S6). The HET-Q1(1-238) construct reduced strongly the number of viable transformants resulting in a viability rate lower than 10% in comparison with transformations with full-length HET-Q1 (*SI Appendix*, Fig. S6). The transformation efficiencies with HET-Q1(1-239) were only slightly decreased, while the HET-Q1(1-237) construct produced a similar number of viable transformants to full-length HET-Q1 (*SI Appendix*, Fig. S6). These results suggest that the cleavage of HET-Q1 occurs after the residue F238 and confirm that proteolysis of HET-Q1 is necessary for the induction of cytotoxicity.

Proteolytic Activity of the Subtilisin-Like Protease HET-Q2 Is Essential for Gasdermin Cytotoxicity. We reasoned that HET-Q2 might be constitutively active (or alternatively be specifically activated by the interaction with HET-Q1) and that its proteolytic activity controls the cell death reaction, likely by direct cleavage of HET-Q1. We therefore generated three *het-Q2* mutants, replacing each of the residues forming the catalytic triad of HET-Q2 (D35, H105, and S266) with an alanine amino acid residue. The mutant alleles (*het-Q2-D35A*, *het-Q2-H105A*, and *het-Q2-S266A*) were introduced into the Δ*het-Q* background, and transformants were tested for barrage formation with the *het-Q1* tester strain. While ∼76% of transformants with wild-type *het-Q2* produced a barrage reaction with the *het-Q1* strain, transformants with mutant *het-Q2* alleles showed reduced or abolished cell death–inducing activity (Fig. 3*A*). The strains transformed with two of the mutants—*het-Q2-H105A* and *het-Q2-S266A*—were unable to trigger cell death with a *het-Q1* strain, while only ∼37% of transformants with the *het-Q2-D35A* allele produced a barrage reaction (Fig. 3*A*). The decrease of activity shown by *het-Q2-D35A* was statistically significant and consistent with previously reported residual protease activity for an equivalent mutation in a human subtilisin (31). These results demonstrate that the proteolytic activity of HET-Q2 is necessary for the control of the HET-Q1–dependent cell death reaction.

Next, we decided to use *S. cerevisiae* as a heterologous system in which to reconstitute the HET-Q1/HET-Q2 cell death reaction. We reasoned that cell death signaling pathways between the yeast and *Podospora* are unlikely to be conserved, as the two fungal species are phylogenetically very distant and differ in cellular organization (unicellular versus multicellular). None of the known components of *P. anserina* allorecognition pathways has homologs in yeast. We coexpressed HET-Q1 and HET-Q2 in yeast. The *het-Q1* gene was under the control of a constitutive promoter, while *het-Q2* was under a galactose-inducible *gal1* promoter. The experiments were performed at 30 °C, the optimal growth temperature for *Saccharomyces*. We found that coexpression of HET-Q1 and HET-Q2 strongly affected the growth of *S. cerevisiae* (Fig. 3*B*). Expression of HET-Q1 alone or HET-Q2 alone did not alter the growth of *S. cerevisiae* nor did the HET-Q2-D35A mutant when coexpressed with HET-Q1 (Fig. 3*B*). The coexpression of the protease and the gasdermin in liquid media also resulted in a population of damaged or dead cells as revealed by the

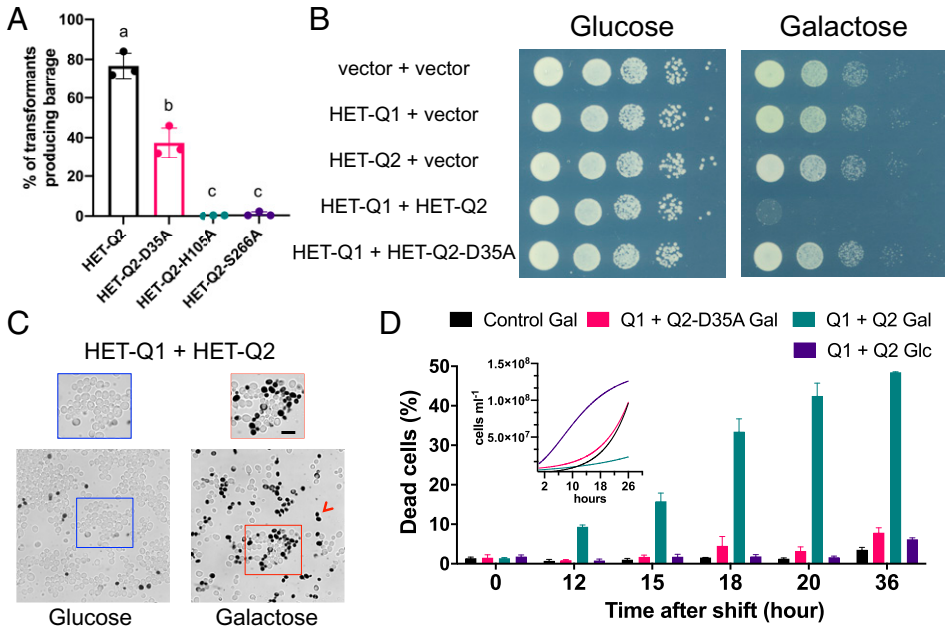

Fig. 3. The proteolytic activity of the subtilisin-like protease HET-Q2 is essential for gasdermin cytotoxicity. (*A*) Quantification of cell death (barrage) induction by transformants expressing HET-Q2 and mutant HET-Q2 variants. Alanine substitutions of residues forming the predicted catalytic triad of HET-Q2 (D35A, H105A, and S266A) affect the cell death reaction. The experiments were performed in triplicate with 50 transformants per experiment. *P* value (a ≠ b ≠ c) < 0.0001, one-way ANOVA with Tukey's multiple comparisons test. (*B*) *S. cerevisiae* drop test on repressed (glucose) and inducible (galactose) growth media. Coexpression of HET-Q1 with HET-Q2 leads to growth arrest of *S. cerevisiae*, while individual expression of both proteins or coexpression of the gasdermin with a catalytically affected protease variant (HET-Q2-D35A) did not affect yeast growth. (*C*) Methylene blue vital dye coloration of yeast cells coexpressing HET-Q1 and HET-Q2 in inducible conditions (galactose) or repressive conditions (glucose). Damaged or dead cells are colored blue (red arrowhead). (Scale bar, 10 μm.) (*D*) Quantification of cell death in yeast cultures. Cell death was measured by counting methylene blue–positive cells at different time points after cultures were shifted to grow in galactose (Gal) inducible conditions. The population of dead cells increased with time up to ∼50% in cell cultures coexpressing HET-Q1 and HET-Q2 (Q1 + Q2 Gal), beginning at ∼10 h post-shift. This time point corresponded to the initiation of growth (inserted panel) in galactose-supplemented media. Methylene blue–positive cells remained below 10% in cultures coexpressing HET-Q1 with a catalytically inactive mutant variant of HET-Q2 (Q1 + Q2-D35A Gal) or in cultures transformed by the empty vectors (Control Gal). Similarly, the population of dead yeast cells remained low in repressive conditions (Q1 + Q2 Glc). The experiments were performed in triplicate.

methylene blue–colored cells observed by microscopy (Fig. 3 *C* and *D*). The percentage of methylene blue–positive cells increased with time in cultures coexpressing HET-Q1 and HET-Q2, peaking at ∼50% after 20 h of growth in galactose-supplemented media (inducible conditions) (Fig. 3*D*). The coexpression of HET-Q1 and HET-Q2 in either noninducible conditions (glucose containing medium) or with the mutant variant HET-Q2-D35A did not affect growth in liquid media, and the population of methylene blue cells remained below 10% at all time points (Fig. 3 *C* and *D*). Taken together, these results suggest that *het-Q1* and *het-Q2* genes constitute an autonomous cell death induction system and further support the direct cleavage of the HET-Q1 gasdermin by the HET-Q2 serine protease.

After reconstituting the *het-Q1*/*het-Q2* cell death reaction in yeast, we used the heterologous setup to probe whether expression of HET-Q1 truncations alone—mimicking the proteolytically activated form of the fungal gasdermin—could trigger cell death. We tested the three HET-Q1 truncations [HET-Q1(1-237), HET-Q1(1-238), and HET-Q1(1-239)] and found that only HET-Q1(1-238) strongly inhibited growth in inducible conditions (galactose) (*SI Appendix*, Fig. S6*C*). Growth in inducible conditions of strains expressing HET-Q1(1-239) appeared only slightly affected, while the HET-Q1(1-237) construct did not show cytotoxicity (*SI Appendix*, Fig. S6*C*). These results reproduce exactly our observations with the three HET-Q1 truncations in *P. anserina*, support the identification of the precise cleavage site (after residue F238), and establish the yeast as a viable tool for studying the mechanism of cytotoxicity of fungal gasdermin-like proteins.

HET-Q1 Induces Pyroptotic-Like Cell Death in a HET-Q2–Dependent Manner in Human HEK 293T Cells. As previously demonstrated for the RCD-1 gasdermin protein (6), we decided to investigate the ability of HET-Q1 to trigger pyroptotic-like cell death in human 293T cells. We thus undertook to reconstitute the HET-Q1/HET-Q2 system in a heterologous setup using 293T cells. The cell cultures were cotransfected with vectors expressing HET-Q1, HET-Q2, or a combination of both fungal proteins. In each cotransfection, the vectors carrying the fungal genes were also expressing the fluorescent proteins GFP (green fluorescent protein)and mCherry from an internal ribosomal entry site sequence present downstream of the *het-Q1* or *het-Q2* genes. We quantified cell death in different cell cultures using flow cytometry by measuring the population of double-positive (GFP+/mCherry+) cells posttransfection (Fig. 4 and *SI Appendix*, Fig. S7). The cell cultures transfected simultaneously with the HET-Q1 gasdermin, and the HET-Q2 protease (in a 1:1 ratio) showed a significant decrease of double-positive (GFP+/mCherry+) cells when compared with cultures transfected only with the gasdermin or only with the protease (Fig. 4*B* and *SI Appendix*, Fig. S7). We examined microscopically the HET-Q1/HET-Q2 cotransfected cell cultures and observed balloon-shaped dead cells reminiscent of cells undergoing pyroptosis (Fig. 4*A*). The samples cotransfected with the gasdermin, and a proteolytically inactive HET-Q2-D35A (or HET-Q2-S266A) variant contained few pyroptotic-like dying cells, and viability was restored to levels of cell cultures transfected with the protease alone (Fig. 4*B*). Similarly, substituting the phenylalanine (F238)—a key amino acid residue for the proteolytic activation of HET-Q1—with an alanine abolished cell death in cultures in which the mutant variant (HET-Q1-F238A) was coexpressed with HET-Q2 (Fig. 4). These results indicate that the HET-Q1/HET-Q2 cell death reaction can be reconstituted in human 293T cells, where the fungal gasdermin HET-Q1 induces pyroptotic-like cell death. Our findings are consistent with the previously observed pyroptotic-like cell death induced in human cells by the RCD-1 fungal gasdermin from the filamentous ascomycete *N. crassa* (6).

Genomic Clustering of *het-Q1* Homologs with Protease-Encoding *het-Q2*–Like Genes in Fungi. Gasdermin-encoding *het-Q1* homologs are ubiquitous in Ascomycota and have been identified in more than 180 fungal species (6, 22). The uncovered functional relation between HET-Q1 and the HET-Q2 protease as well as the previously reported genomic clustering of regulation and cell death execution modules in fungal necroptosis-like pathways (5, 32) prompted us to analyze the local genomic landscape of *het-Q1* homologs in fungi. We retrieved 1,884 *het-Q1* homologs situated in the genomes of 401 fungal species using *P. anserina het-Q1* as a query sequence. We found that 80% of

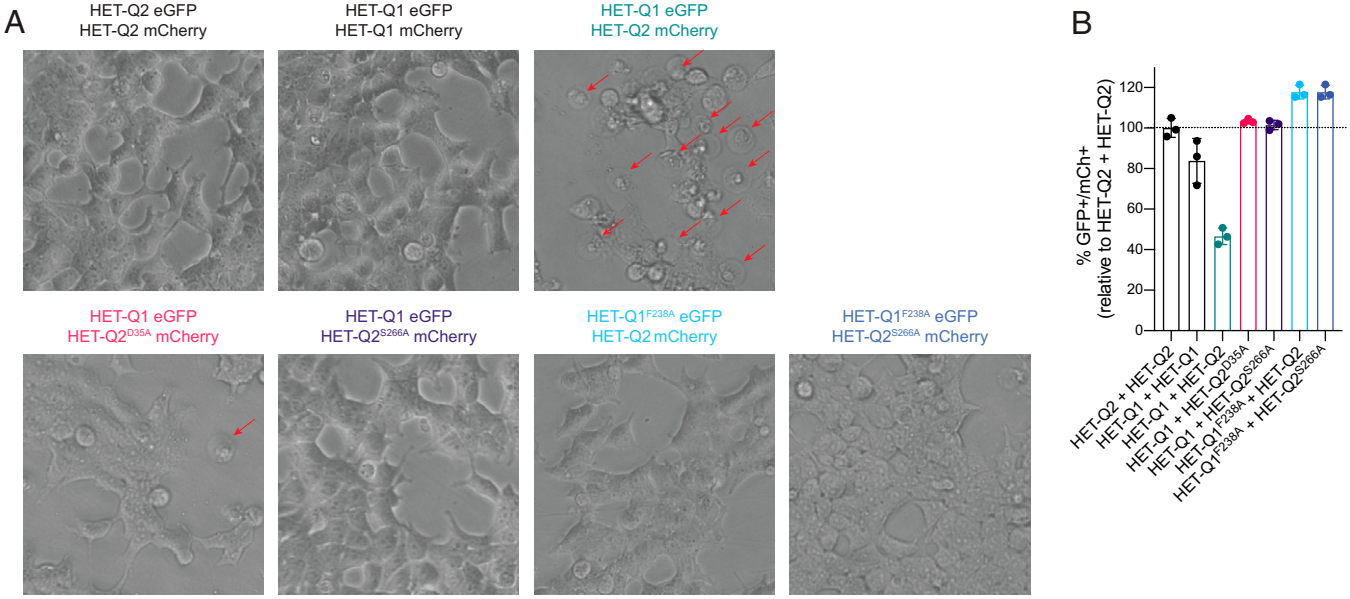

Fig. 4. Coexpression of HET-Q1 and HET-Q2 induces pyroptotic-like cell death in human cells. (*A*) Bright-field images of human 293T cells at 24 h post-transfection with combinations of eGFP-tagged HET-Q1 and mCherry-tagged HET-Q2 wild-type and mutant plasmids. Pyroptotic-like cells are indicated with red arrows. (*B*) Quantification of mCherry and eGFP double-positive cells at 48 h post-transfection analyzed by flow cytometry. The percent of double-positive cells are calculated relative to the protease only, HET-Q2 mCherry + HET-Q2 eGFP, control.

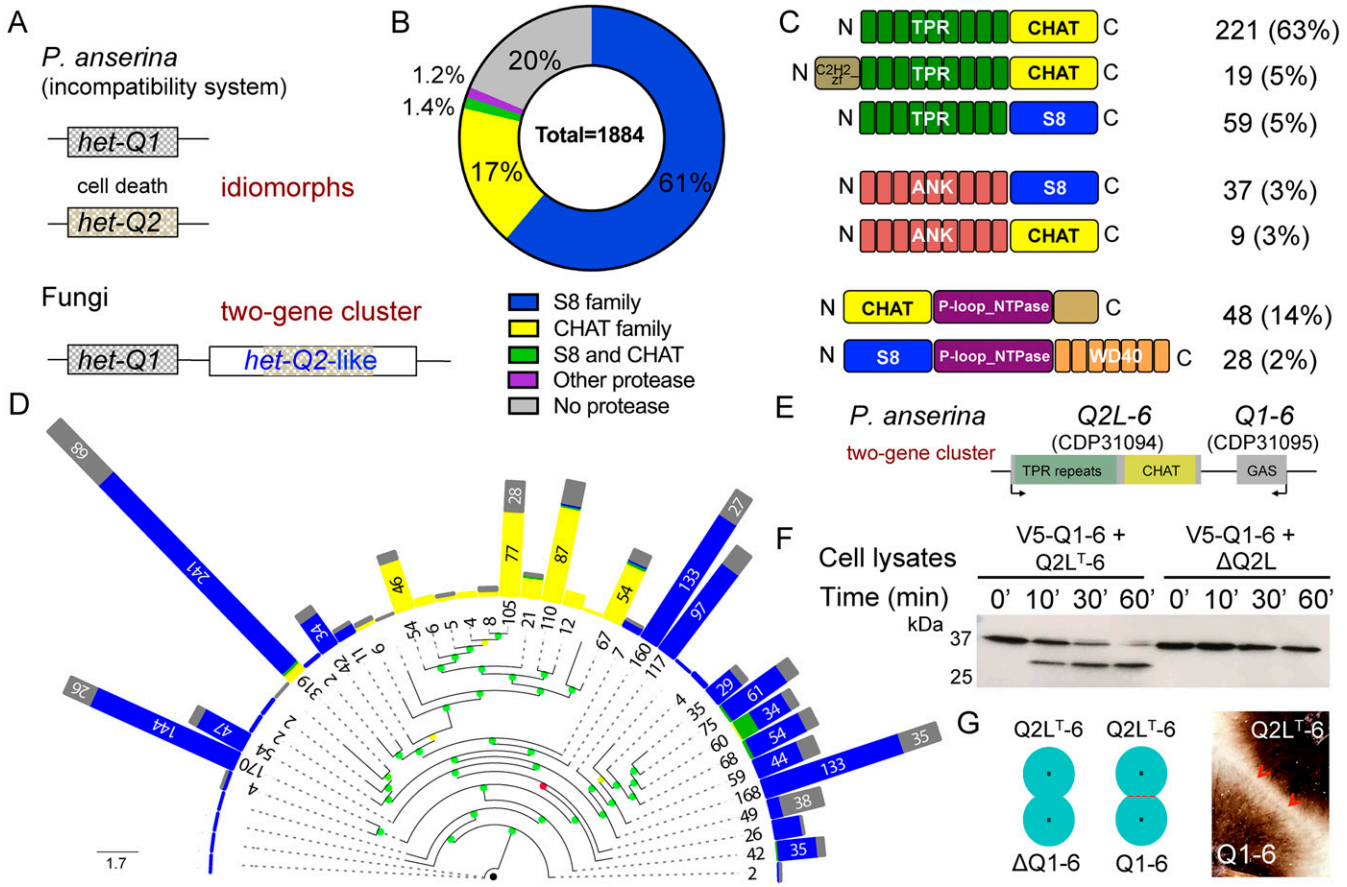

Fig. 5. Gasdermin *het-Q1* homologs are genomically clustered with protease-encoding *het-Q2*–like genes in filamentous fungi. (*A*) A cartoon representation of *het-Q1*/*het-Q2* gene idiomorphs, defining the allorecognition cell death reaction in *P. anserina* and of *het-Q1*/*het-Q2*–like gene clusters, distributed broadly in fungi. (*B*) The percentage of gasdermin homologs situated in the vicinity (10 kbp upstream and downstream) of protease-encoding *het-Q2*–like genes. (*C*) Cartoons representing annotated HET-Q2–like protein architectures. Given are the numbers of proteins in each category and the percentage that each category represents from the total number of CHAT- or S8-containing HET-Q2–like proteins. (*D*) Maximum likelihood phylogenetic tree of *het-Q1* genes. Numbers of *het-Q1* homologs in collapsed branches are shown for each branch. Branch support is color-coded: red—0.00, yellow—0.50, grass-like green—0.75, green—1. Colored bars at tip of branches show the type of protease domain found on the clustered HET-Q2–like proteins (blue—S8 family, yellow—caspase-like CHAT family, green—both) or the number of het-Q1 homologs not clustered with an *het-Q2*–like gene (gray). (*E*) A cartoon showing the two-gene cluster from *P. anserina*, comprising the TRP–CHAT-encoding *Q2-like–6* gene and the gasdermin-encoding *Q1-6* gene. Arrows show the direction of transcription of the genes. (*F*) Western blot showing accumulation of processed V5-Q1-6 in a $Q2L^T$-6–dependent manner. Cell lysates from V5-Q1-6–expressing strain were mixed and incubated (up to 60 min) with cell extracts from a Δ*Q2L-6* strain or from a strain expressing the caspase-like CHAT domain of Q2L-6 ($Q2L^T$-6). The V5-labeled gasdermin protein was proteolytically processed in a time-dependent manner only in the presence of $Q2L^T$-6 (V5-Q1-6 + $Q2L^T$-6 mixture), while V5-Q1-6 remained unprocessed and appeared as single band at the expected size for the full-length protein (~35 kDa) in mixtures with a strain not expressing $Q2L^T$-6 (V5-Q1-6 + ΔQ2L-6 mixture). (*G*) $Q2L^T$-6 transformants were able to produce a barrage reaction (localized cell death) with transformants expressing the Q1-6 gasdermin (red arrowheads). Cartoons represent fusing fungal colonies with a red dotted line representing the barrage reaction, which in some cases was partial (attenuated).

the *het-Q1* genes had at least one gene encoding for a protein with a protease domain as a close neighbor (within 10 kbp) (Fig. 5 *A* and *B* and Dataset S1). Such genes were frequently adjacent to the gasdermin-encoding *het-Q1* homologs—forming two-gene clusters—and were termed *het-Q2*-like (Fig. 5*A*). Approximately 63% (1,187) of the analyzed 1,884 fungal gasdermins were clustered with *het-Q2*–like genes encoding proteins with a putative S8 serine protease domain as found in HET-Q2 (Fig. 5*B*). Remarkably, another 19% (353) of the *het-Q1* homologs were in the vicinity of a *het-Q2*–like gene encoding for a protein with a predicted protease domain of the CHAT (caspase HetF associated with tetratricopeptide repeats [TPRs]) clade, which belongs to the same protease family as the mammalian caspases (33). We also found that 20% (373) of the *het-Q1* homologs were not situated near a *het-Q2*–like gene, yet the vast majority of *het-Q1* genes in this category (76%) were from fungal genomes containing at least one *het-Q1*/*het-Q2*–like two-gene cluster (Dataset S1). Overall, we identified 1,617 *het-Q1*/*het-Q2*–like clusters (1,417 *het-Q1*/*het-Q2*–like gene pairs and 88 *het-Q1*/two *het-Q2*–like three-gene clusters) from 366 fungal species, with a dozen of species carrying at least 10 such clusters in their genomes (Dataset S1). Noteworthy, we also found two distant *het-Q1* homologs [Pa_6_6615 (Q1-6) and Pa_5_3510 (Q1-5)] in the genome of *P. anserina*, clustered with *het-Q2*–like genes, one being of the S8 type, the other of the CHAT type (*SI Appendix*, Fig. S8 and Dataset S1). Neither Q1-6 nor Q1-5 were proteolytically processed by HET-Q2 (*SI Appendix*, Fig. S9), indicating that the products of the two *het-Q1* homologs do not interfere in the *het-Q1*/*het-Q2* allorecognition reaction in *P. anserina* and suggesting that distinct proteolytic specificities control the cytotoxicity of these fungal gasdermins.

The fungal gasdermins show a considerable phylogenetic diversity and formed more than 20 well-supported clades (support values above 0.9 for majority of nonsingleton branches) comprising between 10 and 320 *het-Q1* members (Fig. 5*D*).

Although exceptions occurred, each clade or superclade was predominantly associated with either the S8 or CHAT protease type (Fig. 5*D*). This observation underscores further the functional link between the clustered genes and suggests that gasdermin and protease-encoding genes spend considerable evolutionary time in association while the occasional reassociation with a distinct protease type can occur.

To gain insight into the functional role of these cell death pathways, we analyzed the domain architectures of the HET-Q2–like proteins (Fig. 5*C* and Dataset S2). In the set of 1,601 HET-Q2–like protein sequences, 1,499 (93%) carry N (1,374) or C termini (125) longer than 100 amino acids in addition to the S8/CHAT protease. Using Pfam profiles, we annotated 493 of the 1,499 long N and C termini (33%). The vast majority of the annotated sequences (above 95%) belonged to 16 Pfam clans and resulted in 18 potential protein architectures of HET-Q2–like proteins (Fig. 5*C* and Dataset S2). Several of the most abundant HET-Q2–like protein architectures presented annotated domains consisting of tandem-repeat motifs (TPR, ANK [ankyrin], or WD40 repeats), which are known to mediate protein–protein interactions and/or ligand-binding functions (34) (Fig. 5*C*). Furthermore, we found that some of the *het-Q2*–like genes encode for nucleotide-binding and oligomerization (NOD)-like receptors (NLRs), exhibiting a typical tripartite domain organization with a central P-loop containing the NOD domain flanked by the protease domain and tandem-repeat motifs (specifically S8/NACHT/WD40) (Fig. 5*C*). Overall, our analyses indicate that the majority of fungal gasdermins are clustered with genes encoding for putative CHAT or S8 protease domain-containing, multidomain proteins, some of which belong to a class of cell death–controlling innate immunity receptors.

To investigate the regulation of the fungal gasdermins by the genomically clustered *het-Q2*–like protease-encoding genes, we decided to work with a two-gene cluster from *P. anserina* (Fig. 5*E*). The gene cluster, situated on chromosome six, comprises a *het-Q1* homolog (Pa_6_6615, named Q1-6) and a *het-Q2*–like gene (Pa_6_6610, named Q2L-6), which encodes N-terminal TPR repeats and a C-terminal caspase-like CHAT domain (Fig. 5*E*). Reasoning that the Q2L-6 protein might be in an inactive, repressed state, we decided to work only with the protease domain, encompassing residues 701 to 1,005 of Q2L-6, and thus engineered a truncated $Q2L^{T}$-6 allele. The $Q2L^{T}$-6 construct and the Q1-6 gasdermin were introduced in a Δ*het-Q* Δ*Q1-6* Δ*Q2L-6* strain under the control of the *het-Q2* and *het-Q1* promoters, respectively, to ensure expression in laboratory conditions. Viable transformants were obtained with both constructs, although the transformation efficiencies were decreased between 25 to 40% in comparison with the control (*SI Appendix*, Fig. S10). Some Q1-6 transformants produced a barrage reaction (localized cell death) with $Q2L^{T}$-6 transformants (Fig. 5*G*). Furthermore, V5-labeled Q1-6 was processed in a time-dependent manner only in cell lysate mixtures containing $Q2L^{T}$-6 (Fig. 5*F*). These results demonstrate the functional unity of the uncovered *het-Q1*/*het-Q2*–like gene clusters.

Based on these findings, we postulate that fungal gasdermins are, in general, regulated by proteolytic cleavage by HET-Q2–like functional partners (encoded by a closely linked gene) and are an essential part of broader, diverse, and widespread signaling pathways in fungi (Fig. 6). The genomic clustering of the gasdermin genes and the gene encoding their putative cognate protease is highly reminiscent of the clustering of HeLo domain cell death execution proteins with their cognate regulatory amyloid signaling NLR (32, 35). In this context, it is noteworthy that the number of gasdermin homologs and Helo domain pore-forming toxin homologs in fungal genomes are correlated (Pearson's $r = 0.65$, P value < 1e-55, Spearman's $\rho = 0.49$, and P value < 1e-27) (Dataset S3), suggesting that the lifestyle of certain species calls for a high number of parallel RCD pathways.

Discussion

In this study, by molecularly characterizing a fungal allorecognition system from *P. anserina*, we show that fungal gasdermin-like proteins are controlled by proteolytic cleavage, similar to their mammalian counterparts (13, 14). We uncovered that the fungal gasdermin HET-Q1 is proteolytically processed in the presence of the serine protease HET-Q2 during the allorecognition process in *P. anserina*. The proteolytic cleavage removes a ∼5-kDa C-terminal fragment, which unleashes the cytotoxic activity of HET-Q1. We reconstituted the cell death reaction by coexpressing HET-Q1 and HET-Q2 in the yeast *S. cerevisiae* and human 293T cells. The latter finding strongly suggests that the fungal gasdermin is directly processed by the serine protease and establishes the HET-Q1/HET-Q2 protein pair as an autonomous RCD system. In this context, we uncovered by genome mining that ∼80% of the gasdermin-encoding genes in fungi are clustered with *het-Q2*–like genes, encoding proteins with a putative protease domain, which belongs in the majority of cases to the subtilisin-like serine proteases (S8 family). Our analyses also identified that a subset of the HET-Q2–like proteins carry a caspase-related CHAT domain, while others exhibit NLR-like protein architectures. These findings prompted us to propose that, similar to HET-Q1, proteolytic cleavage is the general mode of activation for the fungal gasdermins. Furthermore, we propose that, for the vast majority of HET-Q1 homologs, the proteolysis occurs via an activated HET-Q2–like protein encoded by the gene adjacent to the gasdermin-encoding gene. The genomic clustering of genes encoding pore-forming toxins and the receptors that activate them has been previously reported in fungi in the case of the HeLo domain pore-forming toxins and their cognate NLR receptors (32, 35).

Gasdermin-Regulated Cell Death in the Context of Comparative Immunology. This study extends the evolutionary parallels between fungal and mammalian cell death pathways beyond the previously uncovered conservation of cell death execution modules (gasdermin pore-forming domain). Our findings establish a broader evolutionary framework for gasdermin-regulated cell death by unveiling a common mode of activation (proteolysis) for the gasdermin family in eukaryotes performed by similar types of proteases, which can be associated—at least in some cases—with homologous upstream receptors (NLR proteins) (Fig. 6).

During pyroptosis, the mammalian gasdermins are processed either by caspases (11–13, 36) or, in the case of GSDMB, by a serine protease (GZMA) (20). Serine proteases play a key role in human immunity in which they can control inflammatory and noninflammatory cell death pathways (37). Furthermore, subtilisin-like serine proteases termed *phytaspases* (plant aspartate-specific protease) have been shown to control cell death in plants (38, 39). Phytaspases exhibit caspase-like specificity and can induce immune-related cell death in response to viral infections (40). Our findings now suggest that both types of proteases (subtilisin like and caspase like) regulate gasdermin-dependent cell death in fungi, likely in the context of organismal defense. While metacaspases (41), distantly related to caspases, have been previously shown to control fungal cell death in various physiological and stress conditions (1), our work proposes an unprecedented role for caspase-like domains in fungal non-self–recognition processes.

Besides the significance for the evolution of the proteolytic control of RCD, our work uncovers that, as described in mammals, some gasdermin proteins are downstream of NOD-like receptors or NLR-like proteins. Nevertheless, it appears that, in fungi, the signaling pathways leading to the activation of gasdermin cytotoxicity are less complex with the NLR protein carrying directly the protease domain, while in mammals, the

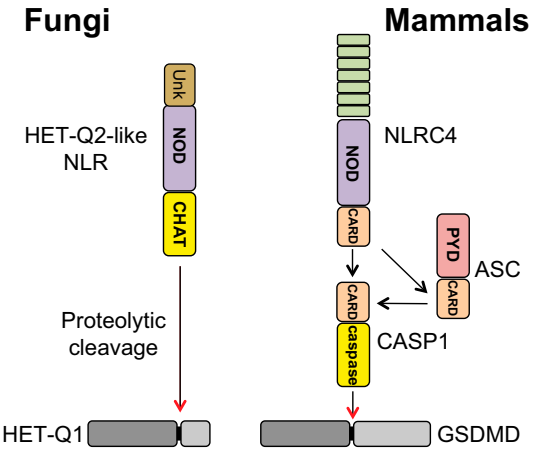

Fig. 6. Comparative models of cell death pathways in fungi and mammals. Shown is an example of a CHAT domain containing fungal NLR-like protein—a HET-Q2–like protein—hypothesized to activate through proteolytic cleavage a downstream HET-Q1 protein. Such HET-Q2–like/HET-Q1 pathways appear analogous to pyroptotic-inducing cell death pathways in mammals. Given example shows the downstream activation of GSDMD (gasdermin D) by NLRC4 (NLR family CARD-containing protein), which can directly activate caspase-1 (CASP1) or indirectly via the ASC protein (apoptosis-associated speck-like protein containing a CARD) (42). PYD—Pyrin domain. Unk—unknown.

NLRs use adapter domains (i.e., CARD—caspase activation and recruitment domain) to activate downstream caspases directly (in some cases) or through adaptor proteins like an apoptosis-associated speck-like protein containing a CARD (Fig. 6) (42).

Remarkably, gasdermin-dependent cell death has recently been reported in bacteria, with several similarities emerging between bacterial and fungal pathways (43). Both fungal and bacterial gasdermins are genomically clustered with genes encoding multidomain proteins containing a protease domain, which regulates the proteolytic cleavage of the gasdermins proteins. The HET-Q2–like proteins in fungi and their bacterial counterparts can carry evolutionarily related protease domains (subtilases or caspase-like CHAT proteases) and, in some cases, belong to the NLR protein family. In addition, similar to bacterial gasdermins, fungal gasdermins carry relatively small inhibitory C-terminal domains (compared with mammalian gasdermins). Although structural details of the inhibited state of fungal gasdermins remain unknown, it is conceivable that gasdermins in fungi and bacteria share a similar molecular mechanism of inhibition. Importantly, the discovery of gasdermin-dependent cell death in bacteria further underscores the ancient origin of this type of cell death, and considering that the bacterial gasdermin clusters are frequently encoded in anti-phage defense islands, it appears that gasdermin-related cell death has been a component of the molecular non-self–discrimination toolkit from the earliest days of natural history.

Allorecognition Systems in Fungi: Branching Out of Broader and Unexplored Cell Death Pathways. Our findings suggest that the *het-Q1*/*het-Q2* allorecognition system found in *P. anserina* has emerged from an ancestral *het-Q1*/*het-Q2*–like two-gene cluster. In this model, genomic rearrangements have resulted in the *het-Q2* gene, which encodes only the protease domain of a HET-Q2–like protein and hence results in a constitutively active protease, triggering cell death when coexpressed with HET-Q1. In this hypothesis, the *het-Q1*/*het-Q2* system would represent an evolutionary exaptation by which a preexisting immune pathway has been refurbished into an allorecognition system (44). A similar evolutionary scenario has been proposed for a two-gene cluster involving an NLR and a different pore-forming toxin (HET-S) in *Podospora*, where a point mutation and a transposon insertion have generated an incompatibility system (*het-s*/*het-S* allelic system) (45). In addition, several other NLR-based allorecognition systems are considered to originate from broader non-self–recognition–dedicated molecular pathways (46). The exaptation model could equally be proposed for the *rcd-1–1*/*rcd-1–2* allorecognition system in *N. crassa* in which genomic rearrangements have been associated with the *rcd-1* locus (22). Our study supports thus further the hypothesis that allorecognition genes originate from preexisting broader signaling pathways, likely involved in the xenorecognition and mediation of interspecific biotic interactions (47).

Conclusion

The present results establish that, in filamentous fungi, in addition to necroptotic-like pathways regulated by amyloid signaling (5), gasdermin-dependent pathways regulated by proteolytic cleavage abound. Mammals and fungi thus share core components and molecular mechanisms of RCD pathways. We hereby critically expand the evolutionary parallels between RCD pathways in two of the major clades of Opisthokonta (fungi and animals). While the extent of the molecular and functional similarities (and differences) remains to be fully explored, our study unveils a remarkable evolutionary conservation in cell death signaling and execution in the context of eukaryotic innate immunity and, as such, represents a further step toward the molecular definition of the fungal immune system.

Materials and Methods

Strains and Plasmids. *P. anserina* strains used in this study were wild-type *het-Q1* and *het-Q2* and the Δ*het-Q1* (Δ*het-Q*) strain. All strains were cultivated at 26 °C using standard procedures. To produce the Δ*het-Q* strain, we replaced the *het-Q1* ORF (Pa_7_10775) with the *nat1* gene, encoding a nourseothricin acetyl transferase, procuring resistance to the nourseothricin antibiotic. The *het-Q1* deletion cassette consists of the *nat1* gene flanked by the upstream and downstream regions of the *het-Q1* gene. To produce the deletion cassette, we amplified 1,055 bp (base pair) upstream of *het-Q1* ORF using primers 5′-AATATTGGAGAAGCAAAATGAGGC-3′ and 5′-TTTAGGTTCTTCTGAAAAGAGATAC-3′ and cloned the PCR fragment upstream of the *nat1* gene. Downstream of the *nat1* gene, we cloned a PCR fragment corresponding to 894 bp downstream of Pa_7_10775, starting from the stop codon of the gene. The PCR fragment was amplified with the primers 5′GAGGAAGGTTATAATCGATGTGTG-3′ and 5′-GCAGTGGCGTTTGTCTTCGC-3′. The *het-Q1* deletion cassette was constructed into a pBlueScript II–derived vector (termed "p1"). To delete the *het-Q1* gene, we used 5 μg 2.76 kbp *NcoI*-linearized 10,775::nat1 (deletion cassette) DNA fragment, which we introduced into a *het-Q1* Δ*PaKu70* strain. Nourseothricin-resistant transformants were selected, screened by PCR and backcrossed with the wild-type reference strain to obtain Δ*het-Q* homokaryons. The barrage phenotype segregated with the nourseothricin-resistance phenotype in the progeny with resistant transformants unable to produce a barrage reaction with a *het-Q2* strain.

The *het-Q1* gene was amplified with primers 5′-GTGTTTCGCTTGTTCAATCCG-3′ and 5′-TTTTCACAATGGAAATCGGGATG-3′, and the 1.85-kbp PCR fragment was cloned with *EcoRV* into a pBlueScript-derived vector carrying the hygromycin-resistance *hph* gene. Similarly, we amplified the *het-Q2* gene using primers 5′-AACATATATATATGCTGTCCCGAC-3′ and 5′-TTTTCACAATGGAAATCGGGATG-3′, and the PCR fragment (2.45 kbp) was cloned with the *EcoRV* restriction enzyme into the SKhph vector. The final constructs were sequenced, and the vectors (SKhph, SKhph-Q1, and SKhph-Q2) were used for viability reduction assays.

To construct the Δ*het-Q1* Δ*Q1-6* Δ*Q2L-6* strain, we replaced the *Q1-6* and *Q2L-6* two-gene cluster with the *nat1*-encoding cassette, procuring resistance to nourseothricin. To produce the deletion cassette, we amplified the promoter region (836 bp) of *Q2L-6* using 5′-CCAACCGTTAGATGAACGACG-3′ and 5′-CTCCTCTAATGGTTGGTTGGTG-3′ and the promoter region (870-bp) of *Q1-6* with primers 5′-GTTGAACTTGTTGGGGGTTGC-3′ and 5′-TTGGCGAGGGCGGTTTGGATG-3′ and cloned these regions upstream and downstream of the *nat1* resistance gene, and the resulting cassette was then used to delete the two-gene cluster.

For the heterologous expression of *het-Q1* and *het-Q2* in the yeast *S. cerevisiae*, the coding sequences of the two genes were PCR amplified and cloned

in the pRS413 (48) and pGal vectors, respectively. The *het-Q1* sequence was amplified with primers 5′-TTGGATCCATGCCCACCAAAACCTCCCAAC-3′ and 5′-GGTCGACTCACGCCTTGGCAGCAACATC-3′, carrying *BamHI* and *SalI* restriction sites. The 853-bp PCR fragment was cloned in the pRS413 vector digested with *BamHI* and *XhoI* to obtain the pRS413-het-Q1 plasmid. The *het-Q1* sequence was under the control of the strong constitutive promoter of the glyceraldehyde-3-phosphate dehydrogenase gene. The *het-Q2* coding sequence was cloned under the control of a galactose-inducible promoter (*gal1*), using "gap repair" methods (49), to produce the pGal-het-Q2 plasmid.

Site-directed mutagenesis was performed with a QuikChange II kit (Agilent) using manufacturer recommended procedures.

Mapping and Positional Cloning of *het-Q1* and *het-Q2*. To identify the *het-Q* locus and clone the *het-Q1* and *het-Q2* genes, we first undertook a classical genetics mapping to situate more precisely the locus on chromosome 7. For this, we crossed a *P. anserina het-Q2* strain with a *het-Q1* Δ*PaATG1* strain (*PaATG1::hph)* in which the *PaATG1* is replaced with a hygromycin-resistance cassette. The *PaATG1* gene deletion has been previously described and characterized (25). We isolated 112 uninucleated spores, from which 78 spores germinated. The hygromycin-resistance screen showed that 35 (45%) spores are resistant to the antibiotic, while 43 (55%) are sensitive. Barrage tests (with *het-Q1* and *het-Q2* tester strains) further showed that only two recombinant spores (*het-Q2* Δ*PaATG1*) have been obtained from the 78 germinated spores. Based on the 2.5% of recombination between the *PaATG1* and the *het-Q1* loci and knowing that 1 cM equals ∼25 kbp in *P. anserina*, we calculated that the physical distance between the two loci is ∼62.5 kbp.

To pinpoint the *het-Q* locus, we undertook a "chromosomal walking" approach (50) with cosmids and plasmids carrying DNA from the *het-Q1* strain previously used to sequence *P. anserina* reference genome (S genotype) (51). We used four cosmids [GA0AAD19ZF04 (CQ2), GA0AAD26ZD03 (CQ3), GA0AAD29ZA05 (CQ4), and GA0AAD50ZA08 (CQ5)] and five plasmids [GA0AB158BG07 (Q1), GA0AB263AH07 (Q2), GA0AB26BB11 (Q3), GA0AB218BA11 (Q4), and GA0AB91DC06 (Q5)] encompassing a 200-kbp region around the *PaATG1* (Pa_7_10890) locus. The cosmids were carrying the *hph* gene (hygromycin resistance) and were transformed in a *het-Q2* strain and viable transformants quantified. The transformations were performed with 10 μg cosmid DNA. The plasmids used for the identification of the *het-Q* locus were used in cotransformation with the *hph*-bearing vector pCSN43 (GenBank: LT726869.1) (3:1 ratio for 12 μg total DNA). These viability reduction assays identified the plasmid GA0AAD29ZA05 (CQ4), carrying an 11-kbp insert and containing five genes, as the region where *het-Q1* is situated. Five variables in size deletions were produced, and after viability reduction tests, it was determined that vectors carrying DNA fragments containing the Pa_7_10775 (GenBank: CDP32598.1) gene reduced the number of hygromycin-resistant transformants.

Viability Reduction and Vegetative Incompatibility Assays. The vegetative incompatibility assays (barrage tests) were performed on standard corn meal agar DO medium. Viability assays were performed by the transformation of protoplasts (or spheroplasts) of *P. anserina* strains (52) (of the *het-Q1*, *het-Q2*, or Δ*het-Q* genotypes), with the SKhph, SKhph-Q,1 and SKhph-Q2 vectors carrying the *hph* gene, which procures hygromycin resistance. The transformations were carried with 7.5 or 10 μg vector DNA. Transformants were counted after 6 d of incubation at 26 °C.

***S. cerevisiae* Drop Test Assay and Methylene Blue Coloration.** The pGal-het-Q2, pRS413-het-Q1, and the two vectors (pGal and pRS413) expressing free GFP were cotransformed in *S. cerevisiae* (Y4722, *Mat-a*, *his3Δ1*, *leu2Δ0*, *ura3Δ0*, *trp1::LEU2*) using the one-step transformation protocol (53). Tryptophan and histidine prototrophic transformants were selected and grown in liquid media (10% glucose). Culture suspensions ($1.5.10^7$ cellules/mL) were serially diluted (by a factor of 10), and 5 μl each suspension was spotted on solid SC (synthetic complete) medium without histidine and tryptophan (SC −H −W) with either galactose (2%) or glucose (2%) as a carbon source. The plates were incubated at 30 °C from 3 to 5 d before imaging.

Yeast cells were grown in liquid SC −H −W (10% glucose). The cells were then harvested by filtration (0.45-μ filter), washed with preheated (30 °C) SC −H −W 2% galactose, and then resuspended (6×10^6 cells ml^{-1}) and grown in the same galactose medium at 30 °C under shaking (300 rpm). Methylene blue coloration was done using standard procedures (54). Briefly, cell culture aliquots were mixed 4:1 (vol/vol) with 0.2% of methylene blue (dissolved in tribasic sodium citrate) in 2 mL Eppendorf tubes, repeatedly inverted manually for 30 s, and cells were harvested by centrifugation (45 s, 15,000 × *g*). Dead cells are identified under a microscope and the percentage of methylene blue positive cells calculated.

Cell Culture and Reconstituted Cell Death Assay. Human 293T kidney cells were grown in DMEM (Dulbecco's modified Eagle medium) supplemented with 10% FBS (fetal bovine serum), 100 U/mL penicillin, 100 mg/mL streptomycin, and 2 mM L-glutamine. To reconstitute HET-Q1/HET-Q2–mediated cell death in 293T cells, constructs producing enhanced GFP (eGFP)- or mCherry-tagged HET-Q1 or HET-Q2 were cotransfected using Lipofectamine 2000 (Invitrogen) following the manufacturer's protocol. To quantify mCherry- and eGFP-positive cells, the cells were harvested manually at 48 h post-transfection, washed in PBS (phosphate-buffered saline), and analyzed directly using standard flow cytometry protocols.

Crude Cell Extracts and In Vitro Proteolytic Cleavage of HET-Q1. Protoplasts of different *P. anserina* strains were prepared using standard methods (55) at a final concentration of 10^6 protoplasts/μl. The cell extracts were prepared from 200 μl protoplasts, which were suspended in 10 mM phosphate buffer (Na_2HPO_4, NaH_2PO_4) pH 7.4 after centrifugation at 4 °C, 5,000 rpm for 10 min. Protoplast suspensions were sonicated (at amplitude four with a Soniprep 150) twice for 10 s with 30 s on ice between sonication cycles. Sonicated samples were centrifuged at 4 °C, 10,000 rpm for 10 min, and 160 μl supernatant was transferred to a new Eppendorf tube and kept at 4 °C.

The experiments were carried by mixing 50 μl each crude extract and incubating the reaction mixtures at 26 °C up to 1 h. To stop the reaction at a specific time point, 15 μl crude cell extract mixtures were added to 15 μl 3× protein loading dye (SDS [sodium dodecyl sulfate] 3.4%).

Data Availability. All data from this work are included in the main text and the supporting information of the paper.

ACKNOWLEDGMENTS. The work was funded by recurrent funds from the CNRS and University of Bordeaux. W.D. was supported in part by the National Science Centre of Poland (Grant No. 2015/17/D/ST6/04054). We thank Robert Debuchy for providing the cosmids and plasmids for the cloning of *het-Q1*.

1. A. P. Gonçalves, J. Heller, A. Daskalov, A. Videira, N. L. Glass, Regulated forms of cell death in fungi. *Front. Microbiol.* **8**, 1837 (2017).
2. S. J. Saupe, Molecular genetics of heterokaryon incompatibility in filamentous ascomycetes. *Microbiol. Mol. Biol. Rev.* **64**, 489–502 (2000).
3. D.-X. Zhang, D. L. Nuss, Engineering super mycovirus donor strains of chestnut blight fungus by systematic disruption of multilocus vic genes. *Proc. Natl. Acad. Sci. U.S.A.* **113**, 2062–2067 (2016).
4. F. Debets, X. Yang, A. J. F. Griffiths, Vegetative incompatibility in Neurospora: Its effect on horizontal transfer of mitochondrial plasmids and senescence in natural populations. *Curr. Genet.* **26**, 113–119 (1994).
5. A. Daskalov *et al.*, Identification of a novel cell death-inducing domain reveals that fungal amyloid-controlled programmed cell death is related to necroptosis. *Proc. Natl. Acad. Sci. U.S.A.* **113**, 2720–2725 (2016).
6. A. Daskalov, P. S. Mitchell, A. Sandstrom, R. E. Vance, N. L. Glass, Molecular characterization of a fungal gasdermin-like protein. *Proc. Natl. Acad. Sci. U.S.A.* **117**, 18600–18607 (2020).
7. G. S. Salvesen, A. Hempel, N. S. Coll, Protease signaling in animal and plant-regulated cell death. *FEBS J.* **283**, 2577–2598 (2016).
8. O. Julien, J. A. Wells, Caspases and their substrates. *Cell Death Differ.* **24**, 1380–1389 (2017).
9. H. Y. Chang, X. Yang, Proteases for cell suicide: Functions and regulation of caspases. *Microbiol. Mol. Biol. Rev.* **64**, 821–846 (2000).
10. C. N. LaRock, B. T. Cookson, Burning down the house: Cellular actions during pyroptosis. *PLoS Pathog.* **9**, e1003793 (2013).
11. J. Shi, W. Gao, F. Shao, Pyroptosis: Gasdermin-mediated programmed necrotic cell death. *Trends Biochem. Sci.* **42**, 245–254 (2017).
12. J. Shi *et al.*, Cleavage of GSDMD by inflammatory caspases determines pyroptotic cell death. *Nature* **526**, 660–665 (2015).
13. N. Kayagaki *et al.*, Caspase-11 cleaves gasdermin D for non-canonical inflammasome signalling. *Nature* **526**, 666–671 (2015).
14. R. A. Aglietti *et al.*, GsdmD p30 elicited by caspase-11 during pyroptosis forms pores in membranes. *Proc. Natl. Acad. Sci. U.S.A.* **113**, 7858–7863 (2016).
15. X. Liu *et al.*, Inflammasome-activated gasdermin D causes pyroptosis by forming membrane pores. *Nature* **535**, 153–158 (2016).
16. J. Ding *et al.*, Pore-forming activity and structural autoinhibition of the gasdermin family. *Nature* **535**, 111–116 (2016).
17. L. Sborgi *et al.*, GSDMD membrane pore formation constitutes the mechanism of pyroptotic cell death. *EMBO J.* **35**, 1766–1778 (2016).
18. P. Broz, P. Pelegrín, F. Shao, The gasdermins, a protein family executing cell death and inflammation. *Nat. Rev. Immunol.* **20**, 143–157 (2020).
19. C. Rogers *et al.*, Cleavage of DFNA5 by caspase-3 during apoptosis mediates progression to secondary necrotic/pyroptotic cell death. *Nat. Commun.* **8**, 14128 (2017).
20. Z. Zhou *et al.*, Granzyme A from cytotoxic lymphocytes cleaves GSDMB to trigger pyroptosis in target cells. *Science* **368**, eaaz7548 (2020).

21. Y. Wang *et al.*, Chemotherapy drugs induce pyroptosis through caspase-3 cleavage of a gasdermin. *Nature* **547**, 99–103 (2017).
22. A. Daskalov, P. Gladieux, J. Heller, N. L. Glass, Programmed cell death in *Neurospora crassa* is controlled by the allorecognition determinant *rcd-1*. *Genetics* **213**, 1387–1400 (2019).
23. M. Paoletti, Vegetative incompatibility in fungi: From recognition to cell death, whatever does the trick. *Fungal Biol. Rev.* **30**, 152–162 (2016).
24. K. Esser, "Podospora anserina" in *Bacteria, Bacteriophages, and Fungi*, R. C. King, Ed. (Springer US, Boston, MA, 1974), pp. 531–551.
25. B. Pinan-Lucarré, A. Balguerie, C. Clavé, Accelerated cell death in Podospora autophagy mutants. *Eukaryot. Cell* **4**, 1765–1774 (2005).
26. N. L. Glass, J. Grotelueschen, R. L. Metzenberg, Neurospora crassa A mating-type region. *Proc. Natl. Acad. Sci. U.S.A.* **87**, 4912–4916 (1990).
27. J. Söding, A. Biegert, A. N. Lupas, The HHpred interactive server for protein homology detection and structure prediction. *Nucl. Acids Res.* **33**, W244–W248 (2005).
28. J. Jumper *et al.*, Highly accurate protein structure prediction with AlphaFold. *Nature* **596**, 583–589 (2021).
29. L. Holm, Using dali for protein structure comparison. *Methods Mol. Biol.* **2112**, 29–42 (2020).
30. M. Hohl, A. Stintzi, A. Schaller, A novel subtilase inhibitor in plants shows structural and functional similarities to protease propeptides. *J. Biol. Chem.* **292**, 6389–6401 (2017).
31. P. Carter, J. A. Wells, Dissecting the catalytic triad of a serine protease. *Nature* **332**, 564–568 (1988).
32. A. Daskalov *et al.*, Signal transduction by a fungal NOD-like receptor based on propagation of a prion amyloid fold. *PLoS Biol.* **13**, e1002059 (2015).
33. L. Aravind, E. V. Koonin, Classification of the caspase-hemoglobinase fold: Detection of new families and implications for the origin of the eukaryotic separins. *Proteins* **46**, 355–367 (2002).
34. K. K. Jernigan, S. R. Bordenstein, Tandem-repeat protein domains across the tree of life. *PeerJ* **3**, e732 (2015).
35. A. Daskalov, M. Paoletti, F. Ness, S. J. Saupe, Genomic clustering and homology between HET-S and the NWD2 STAND protein in various fungal genomes. *PLoS One* **7**, e34854 (2012).
36. S. B. Kovacs, E. A. Miao, Gasdermins: Effectors of pyroptosis. *Trends Cell Biol.* **27**, 673–684 (2017).
37. K. M. Heutinck, I. J. M. ten Berge, C. E. Hack, J. Hamann, A. T. Rowshani, Serine proteases of the human immune system in health and disease. *Mol. Immunol.* **47**, 1943–1955 (2010).
38. N. V. Chichkova *et al.*, Phytaspase, a relocalisable cell death promoting plant protease with caspase specificity. *EMBO J.* **29**, 1149–1161 (2010).
39. S. Reichardt *et al.*, The tomato subtilase family includes several cell death-related proteinases with caspase specificity. *Sci. Rep.* **8**, 10531 (2018).
40. J. Figueiredo, M. Sousa Silva, A. Figueiredo, Subtilisin-like proteases in plant defence: The past, the present and beyond. *Mol. Plant Pathol.* **19**, 1017–1028 (2018).
41. L. Tsiatsiani *et al.*, Metacaspases. *Cell Death Differ.* **18**, 1279–1288 (2011).
42. W. A. Andrade, D. S. Zamboni, NLRC4 biology in immunity and inflammation. *J. Leukoc. Biol.* **108**, 1117–1127 (2020).
43. A. G. Johnson *et al.*, Bacterial gasdermins reveal an ancient mechanism of cell death. *Science* **375**, 221–225 (2022).
44. S. J. Gould, E. S. Vrba, Exaptation—A missing term in the science of form. *Paleobiology* **8**, 4–15 (1982).
45. A. Daskalov, S. J. Saupe, As a toxin dies a prion comes to life: A tentative natural history of the [Het-s] prion. *Prion* **9**, 184–189 (2015).
46. A. Daskalov, W. Dyrka, S. J. Saupe, "6 NLR function in fungi as revealed by the study of self/non-self recognition systems" in *Genetics and Biotechnology*, J. P. Benz, K. Schipper, Eds. (Springer International Publishing, Cham, 2020), pp. 123–141.
47. M. Paoletti, S. J. Saupe, Fungal incompatibility: Evolutionary origin in pathogen defense? *BioEssays* **31**, 1201–1210 (2009).
48. R. S. Sikorski, P. Hieter, A system of shuttle vectors and yeast host strains designed for efficient manipulation of DNA in *Saccharomyces cerevisiae*. *Genetics* **122**, 19–27 (1989).
49. K. R. Oldenburg, K. T. Vo, S. Michaelis, C. Paddon, Recombination-mediated PCR-directed plasmid construction in vivo in yeast. *Nucleic Acids Res.* **25**, 451–452 (1997).
50. W. Bender, P. Spierer, D. S. Hogness, Chromosomal walking and jumping to isolate DNA from the Ace and rosy loci and the bithorax complex in *Drosophila melanogaster*. *J. Mol. Biol.* **168**, 17–33 (1983).
51. E. Espagne *et al.*, The genome sequence of the model ascomycete fungus *Podospora anserina*. *Genome Biol.* **9**, R77 (2008).
52. Y. Brygoo, R. Debuchy, Transformation by integration in *Podospora anserina*. *Mol. Gen. Genet.* **200**, 128 (1985).
53. D. C. Chen, B. C. Yang, T. T. Kuo, One-step transformation of yeast in stationary phase. *Curr. Genet.* **21**, 83–84 (1992).
54. M. Kwolek-Mirek, R. Zadrag-Tecza, Comparison of methods used for assessing the viability and vitality of yeast cells. *FEMS Yeast Res.* **14**, 1068–1079 (2014).
55. S. Ferrer, D. Ramón, J. Salom, E. Vicente, F. Uruburu, Protoplasts from *Podospora anserina*: Isolation, purification, and transformation. *Curr. Microbiol.* **12**, 301–306 (1985).